Int. J. Electrochem. Sci., 7 **(2012)** 9869 - 9880

International Journal of
ELECTROCHEMICAL
SCIENCE
www.electrochemsci.org

Effects of Conductive Carbon on the Electrochemical Performances of $Li_4Ti_5O_{12}$/C Composites

Xiaodong Zheng, Chenchu Dong, Bing Huang, Mi Lu[*]

Clean Energy Research and Development Center, Binzhou University, Binzhou 256603, People's Republic of China
[*]E-mail: lumihit@sina.com

Received: 25 July 2012 / *Accepted:* 2 September 2012 / *Published:* 1 October 2012

The $Li_4Ti_5O_{12}$/C composites were synthesized by a simple solid-state reaction containing conductive carbon of Super-P, BP-2000 or vapor grown carbon fiber (VGCF) with a constant content of 5 wt.%. The X-ray diffraction (XRD) and scanning electron microscopy (SEM) were used to analyze the structures and morphology of the as-prepared samples. The results indicate that the composites show a spinel crystal structure with a reduced particle size and that the aggregation of particles is inhibited by the addition of carbon. The charge/discharge test indicates that the $Li_4Ti_5O_{12}$ containing BP-2000 shows the best electrochemical performance due to highest specific surface area. The results also show that the high rate performance of the composite with VGCF is superior to that with Super-P, indicating that the structure of the carbon, except for the specific surface area, is another factor that affects the high rate performance of the composite.

Keywords: $Li_4Ti_5O_{12}$/C composite; Anode; Lithium-ion batteries; High-rate

1. INTRODUCTION

Spinel $Li_4Ti_5O_{12}$ (LTO) shows a much attractive performance of long cyclic life as anode for lithium-ion batteries used for energy storage, electric vehicles and hybrid electric vehicles. But these applications are encountering the disadvantage of low electric conductivity. Carbon coating is an effective way in improving the conductivity of the LTO, and the carbon sources include sugar [1], coal oil [2], organic polymers and organic acids [3-9]. The addition of conductive carbon black, such as acetylene carbon black [10] or Super P® [11], in the precursor before sintering also improves the rate performance of LTO. The reasons for the improvement are ascribed to the inhibition of the aggregation of the LTO particles and the improvement of the electron conductivity between the inner-particles

[12]. The latter method shows the advantages of higher electronic conductivity, more accurate carbon content addition and easier method for synthesis.

In our previous paper, we have analyzed the effects of carbon content on the electrochemical performance of LTO/C composite [13]. Results showed that the sample with the addition of 5 wt.% Super P® carbon during synthesis and a further 5 wt.% carbon during slurry preparation exhibited the best performance. But there are several types of conductive carbon used in the lithium-ion batteries and some of them show much different physical characteristics. For example, the Super P® and BP-2000 are particles but with much different specific surface area of about 60 and higher than 1200 m^2/g, respectively, while the vapor grown carbon fiber (VGCF) shows a nano-linear morphology with a specific surface area of only 11 m^2/g. These differences may result in different electrochemical performance of LTO/C composites. In this paper, we synthesized the LTO/C composites using these three types of carbon with the optimal content of 5 wt.% determined in our previous paper, but without further carbon addition during slurry preparation, to study the effects of the different types of carbon on the electrochemical performance of LTO/C composites.

2. EXPERIMENTAL SECTION

2.1 Preparation of sample materials

The LTO/C composites with 5 wt.% carbon were prepared as follows. Li_2CO_3 (AR) and TiO_2 (AR) in adequate amount of ethanol with a Li : Ti molar ratio of 0.86 : 1 were mixed by ball milling for 2 h, then the appropriate weight of conductive carbon (Super P®, BP-2000, or VGCF) with a weight ratio of carbon : LTO = 5 : 95 was added in the slurry and ball-milled for a further 2 h. The mixtures were dried at 80 ℃ and then heat-treated at 800 ℃ for 12 h by a tube furnace with the protection of argon, then cooled to room temperature to obtain the final LTO/C composites (denoted as LTO/SP, LTO/BP-2000, LTO/VGCF, respectively).

2.2 Materials characterization

The structures of the as-prepared samples were measured by X-ray diffraction (XRD) (X'pert PRO, Panalytical) using Cu Kα radiation (λ= 0.15406 nm) over the 2θ range from 10° to 90°. The morphology of the samples was observed by a scanning electron microscope (SEM) (S4800, Hitachi) operated at 15 kV.

2.3 Electrochemical measurements

LTO/C composites were mixed with Polyvinylidene fluoride (PVDF) and an adequate amount of N-methyl-2-pyrrolidone with a weight ratio of 9:1 (LTO/C : PVDF). The slurry of the mixtures was prepared by ball-milling for 2 h, then was coated on a copper foil and dried at 90 °C under vacuum for more than 10 h to obtain the electrode for measurement. The cells (CR2025 coin type) were assembled

in an argon-filled glove box (Etelux 2000, China), where both moisture and oxygen levels were kept at less than 1 ppm. The electrolyte used was 1 mol/L $LiPF_6$ in ethylene carbonate and dimethyl carbonate (EC-DMC, 1:1 v/v) and lithium foil was used as the counter electrode. The charge/discharge cycle was performed using a Neware® instrument at 0.1C to 10 C (1C=175 mA/g) rate in the voltage range 2.5-0.5 V.

3. RESULTS AND DISCUSSION

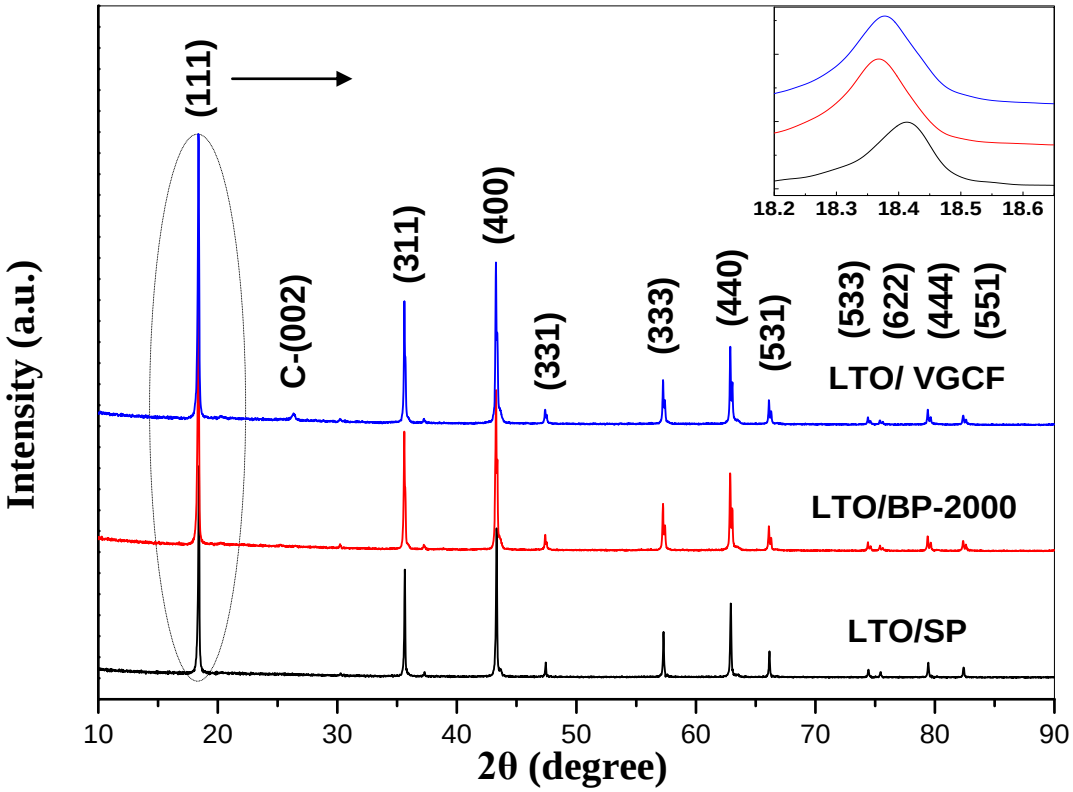

Figure 1. X-ray diffraction patterns of LTO/SP, LTO/BP-2000 and LTO/VGCF

Table 1. The lattice parameter and the average crystalline size of LTO/C composites.

Samples	Lattice parameter, a(nm)	Volume, V(nm^3)	Crystalline size (nm)
LTO/SP	0.8352	582.6	118.9
LTO/BP-2000	0.8357	583.6	79.3
LTO/VGCF	0.8356	583.4	81.0

The X-ray diffraction patterns of the synthesized powders are shown in Figure 1. The crystal structure of each sample is almost in accordance with the $Li_4Ti_5O_{12}$ cubic spinel single phase structure,

except for a weak peak in the pattern of LTO/VGCF at 26.4° (2θ) corresponding to the (002) face of graphite. The peaks of Super P® and BP-2000 are weak due to the small particle size. The fine peaks of $Li_4Ti_5O_{12}$ indicate that the spinel structure is not affected by the addition of carbon during the sintering process.

The enlarged diffraction patterns of the (111) face of the three samples show that the position is shifted to the lower degree in the order of LTO/SP, LTO/VGCF and LTO/BP-2000. Table 1 shows the lattice parameter and the average crystalline size of each sample calculated by the Bragg equation (1) and the Debye-Sherrer formula (2), which is shown as follows:

$$n\lambda = 2\frac{a}{\sqrt{h^2 + k^2 + l^2}}\sin\theta \qquad (1)$$

$$D = \frac{k\lambda}{\beta_{1/2}\cos\theta} \qquad (2)$$

Where a is lattice parameter, n is 1, λ is the wavelength of the X-ray radiation taken 0.15406 nm for Cu Kα, θ is the Bragg angle, h, k and l are Miller indices, D is the crystallite size, k is the Scherer constant taken 0.89, β is the full width half maximum (FWHM) of the diffraction peak measured at 2θ in radians.

According to the Bragg equation, as the position of diffraction peak shifts to smaller angle, the distance between atomic layers becomes larger. During the process of lithium-ion intercalation, the additional lithium-ions enter the octahedral (16c) sites, and lithium-ions initially located at tetrahedral (8a) sites also transport to the octahedral (16c) sites, part of the Ti^{4+} ions transforms to Ti^{3+} ions with larger size [14]. Thus, it can be conclude that larger lattice parameter is beneficial to the migration of lithium-ions and electrons. The intercalation process is described as follows [15]:

$$[Li_3]_{8a}[LiTi_5^{4+}]_{16d}[O_{12}]_{32e} + 3e^- + 3Li^+ \rightarrow [Li_6]_{16c}[LiTi_3^{3+}Ti_2^{4+}]_{16d}[O_{12}]_{32e} \qquad (3)$$

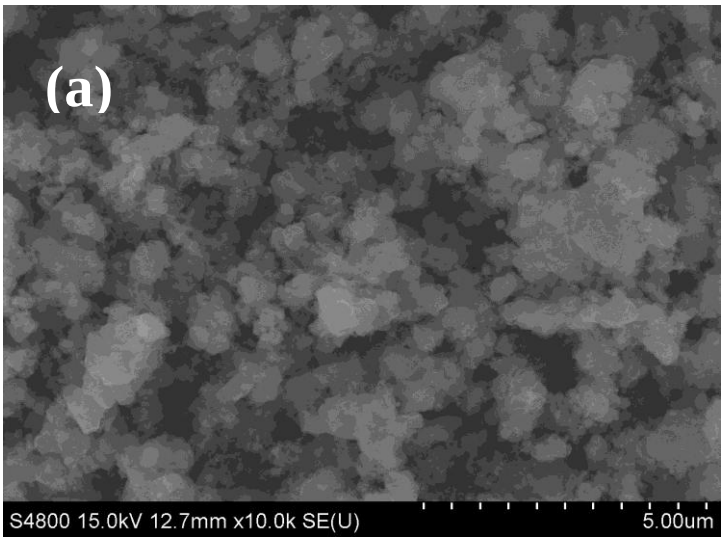

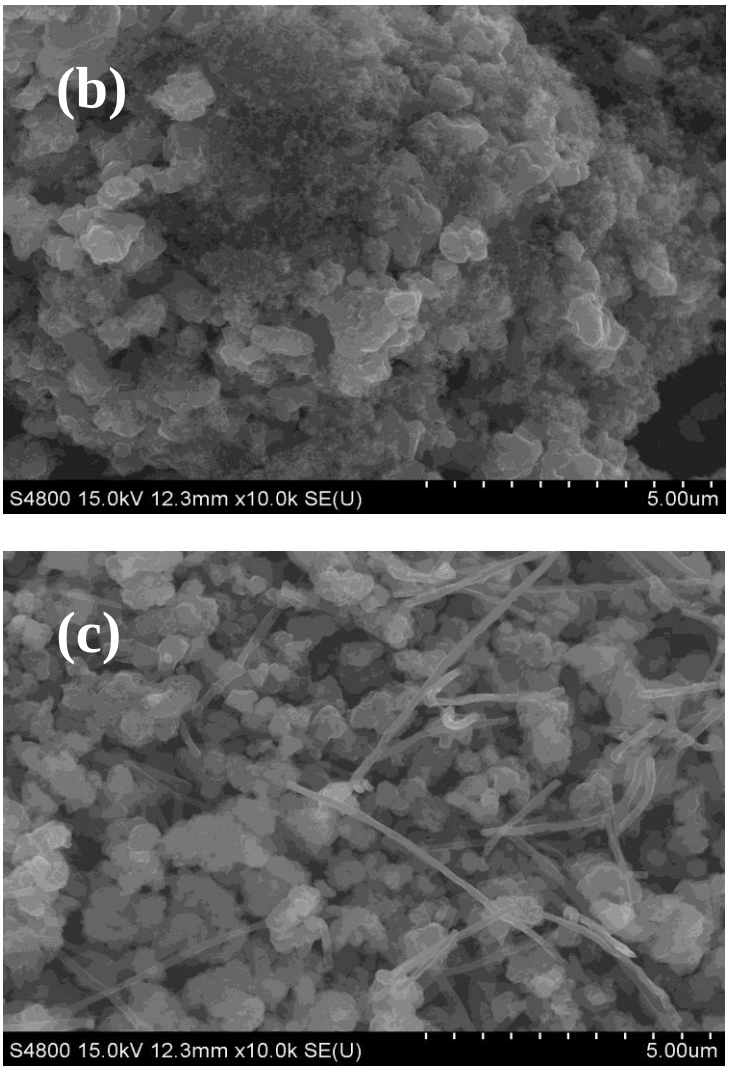

Figure 2. SEM images of the three samples. (a) LTO/SP; (b) LTO/BP-2000; (c) LTO/VGCF

As shown in Table 1, the lattice parameters of LTO/C show an order of $a_{LTO/BP\text{-}2000} > a_{LTO/VGCF} > a_{LTO\text{-}SP}$. The results of the calculated crystalline sizes suggest that BP-2000 and VGCF can inhibit the growth of grain significantly due to the large BET surface area of BP-2000 (1282 m^2/g) and the length of VGCF (10-20 μm).

Figure 2 shows the morphology of the three samples. It shows that the particles of LTO were distributed loosely and homogeneously, and all samples show some extent of aggregation. The morphology of the samples with BP-2000 and Super-P shows similar characteristic: the carbon was distributed homogeneously on the surface of the aggregated particles and among the inter-particles. But the morphology of the sample with VGCF is much difference: the VGCF only distribute between the particles but the aggregation of the LTO particles was also inhibited by VGCF.

Figure 3 shows the cycle performance of each sample at the charge-discharge rates varied from 0.1 to 10 C between 0.5-2.5V. It shows that the charge capacity decreased gradually with the increasing current rate for all samples due to polarization. The LTO/BP-2000 exhibits the best

reversible capacity at all rates, especially from 0.1 to 1 C. The excellent electrochemical performance of LTO/BP-2000 is ascribed to the improvement of the electronic conductivity of the composite and the largest layer space of LTO, which is advantage for the insertion of lithium ions. It is worthy noting that the capacity retention of LTO/VGCF is better than that of LTO/SP during the discharge-charge current rate is increased. This characteristic can be explained as follows: the lithium-ions at high rate are mainly concentrated on the surface of LTO and the three-dimensional conductive network formed by VGCF, which is advantage to the electron transfer between the isolated aggregated-particles. And it can be observed that the gap between samples at 5 C becomes the widest, while at 10 C the reversible capacity of all samples decreased rapidly and the gap approached gradually, which may be ascribed to the rate determining step is changed to lithium ions diffusion in the electrolyte [16]. The capacity retention of LTO/SP, LTO/BP-2000 and LTO/VGCF after above 60 cycles is 91, 99.7 and 98.5%, respectively, which shows that the sample of LTO/BP-2000 shows the best cyclic stability.

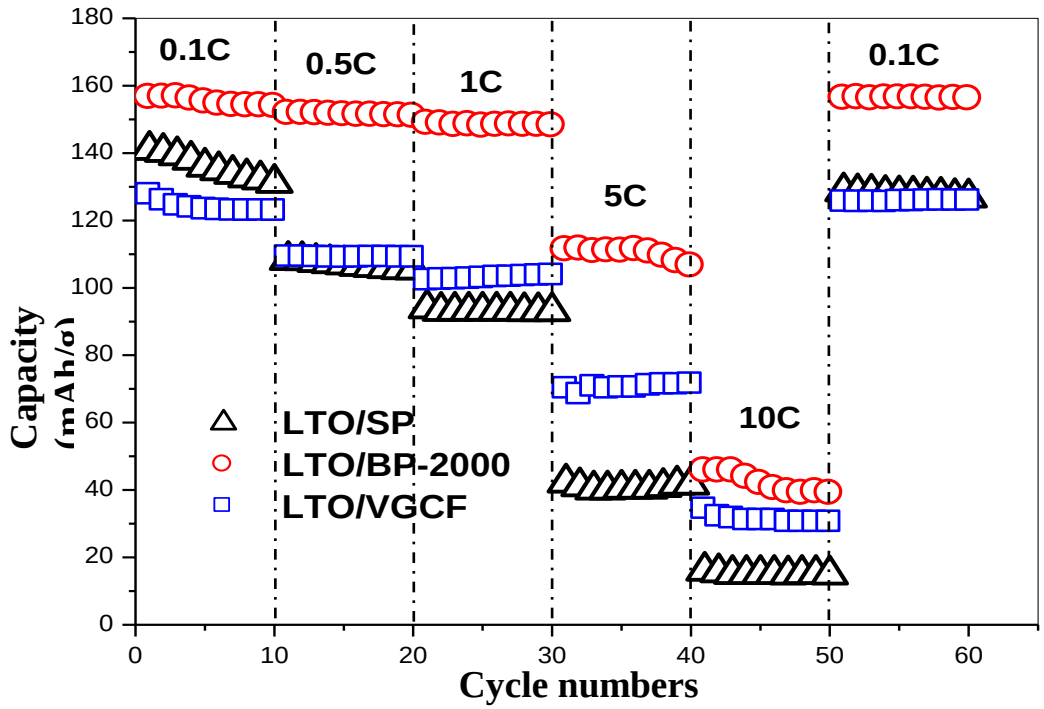

Figure 3. The rate performances of LTO/SP, LTO/BP-2000 and LTO/VGCF cycled at different current rates

Figure 4 shows the initial charge-discharge curves of samples tested at different rates from 0.1 to 10 C, and the inset plot is the initial charge-discharge curves of the corresponding carbon. It shows typical discharge-charge curves of LTO between 2.5-1.0V, showing a discharge plateau at about 1.5V. But the plateaus between 1.0-0.5V in the discharge curves are much different: the potential plateau of LTO/BP-2000 is much longer than the other two samples due to the much larger irreversible capacity of the BP-2000. The irreversible capacity or Coulombic efficiency is related to its specific surface area, which will be covered by solid electrolyte interphase (SEI) layers during the first charge/discharge

process [17], thus the LTO/BP-2000 shows the longest potential plateau between 0.5-1V. Super P, BP-2000 and VGCF are graphite, thus their lithiated potential begins at about 210 mV due to the change of dilute stage-1 to stage-4 [18], resulting in the low reversible capacity of the corresponding carbon. The first charge-discharge cycle of the three carbons is shown as an inset plot in Figure 4. Thus the LTO/BP-2000 shows the lowest initial coulombic efficiency of 68.9% among the three samples. To further analyze the effects of carbon on the power performance of LTO, the differential curves of the corresponding charge-discharge are shown in Figure 5. As shown in Fig. 5 (a)-(c), all samples have a pair of redox peaks (at about 1.53-1.59V) which is attributed to the redox reaction of Ti^{3+}/Ti^{4+} couple, and there is a weak reduction peaks below (or around) 1.0V which can be attributed to the formation of SEI layers on the surface of carbon and LTO.

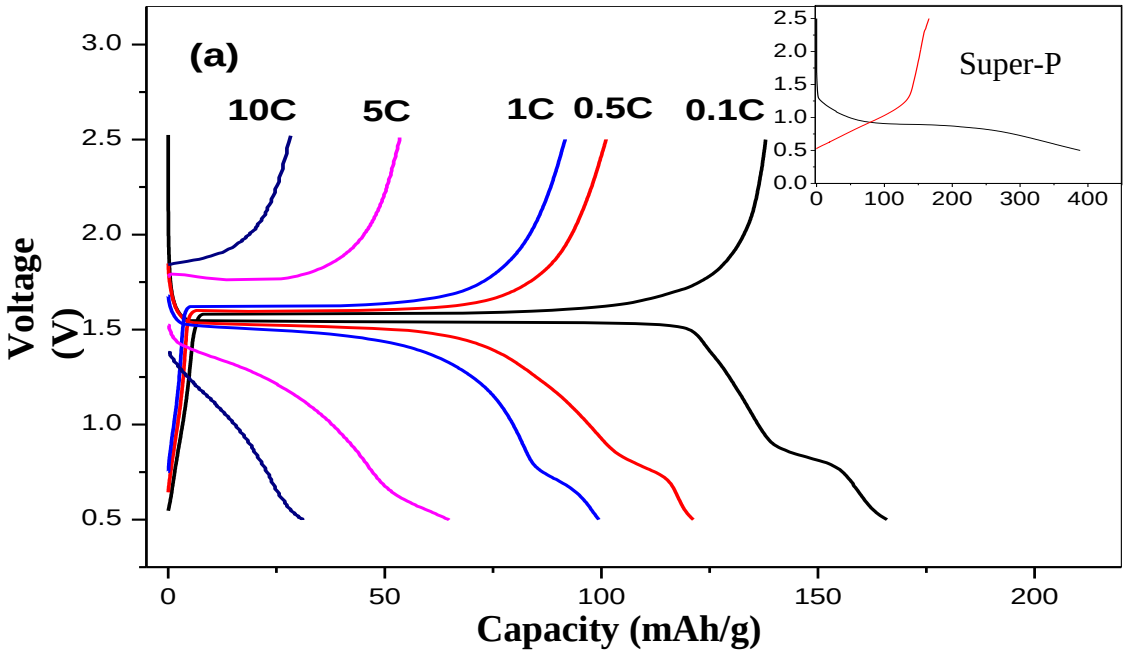

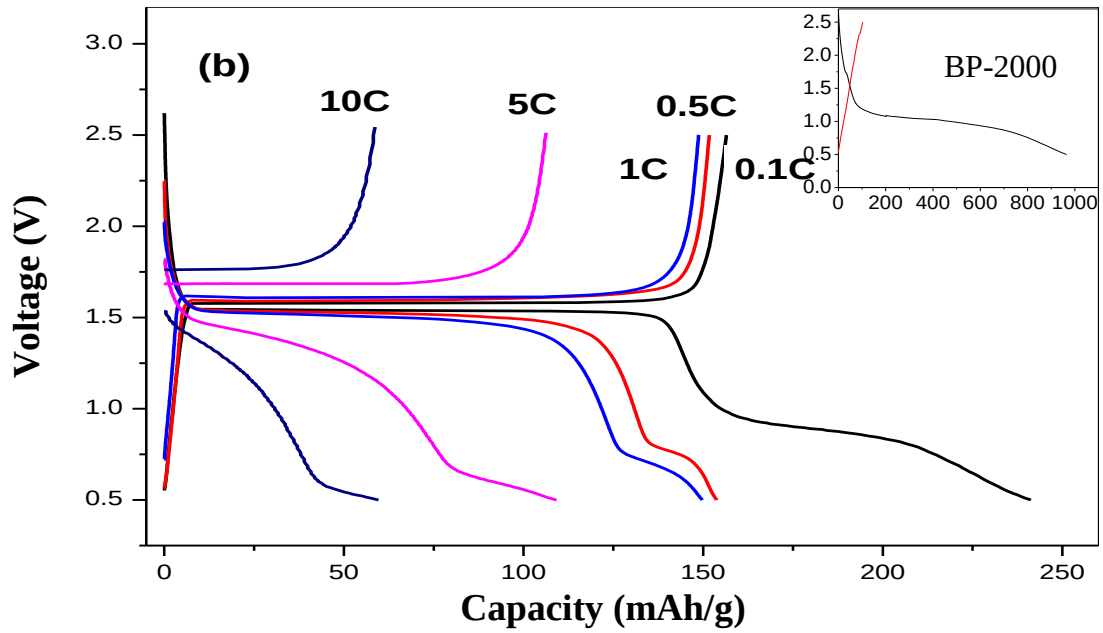

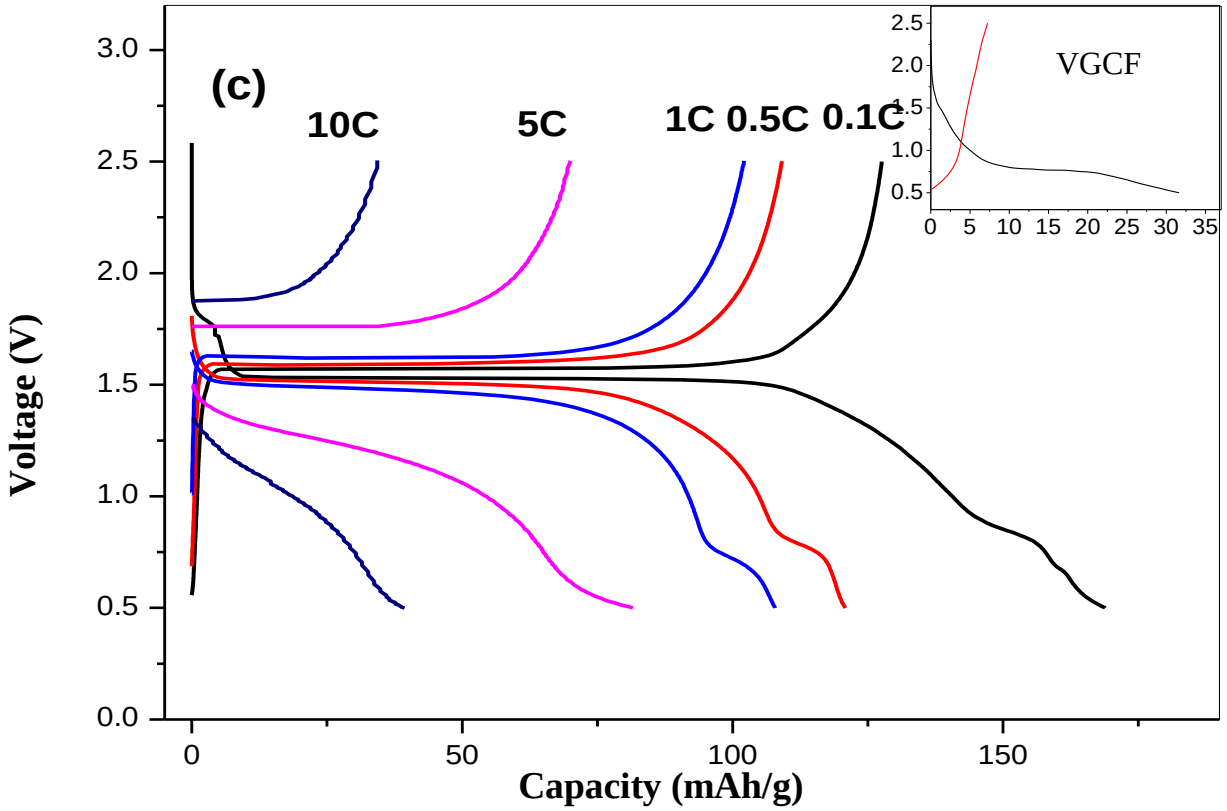

Figure 4. The discharge/charge profiles of the three samples between 0.5V and 2.5V at different current rates. (a) LTO/SP; (b) LTO/BP-2000; (c) LTO/VGCF. The inset plot of the first charge-discharge cycle of the corresponding carbon

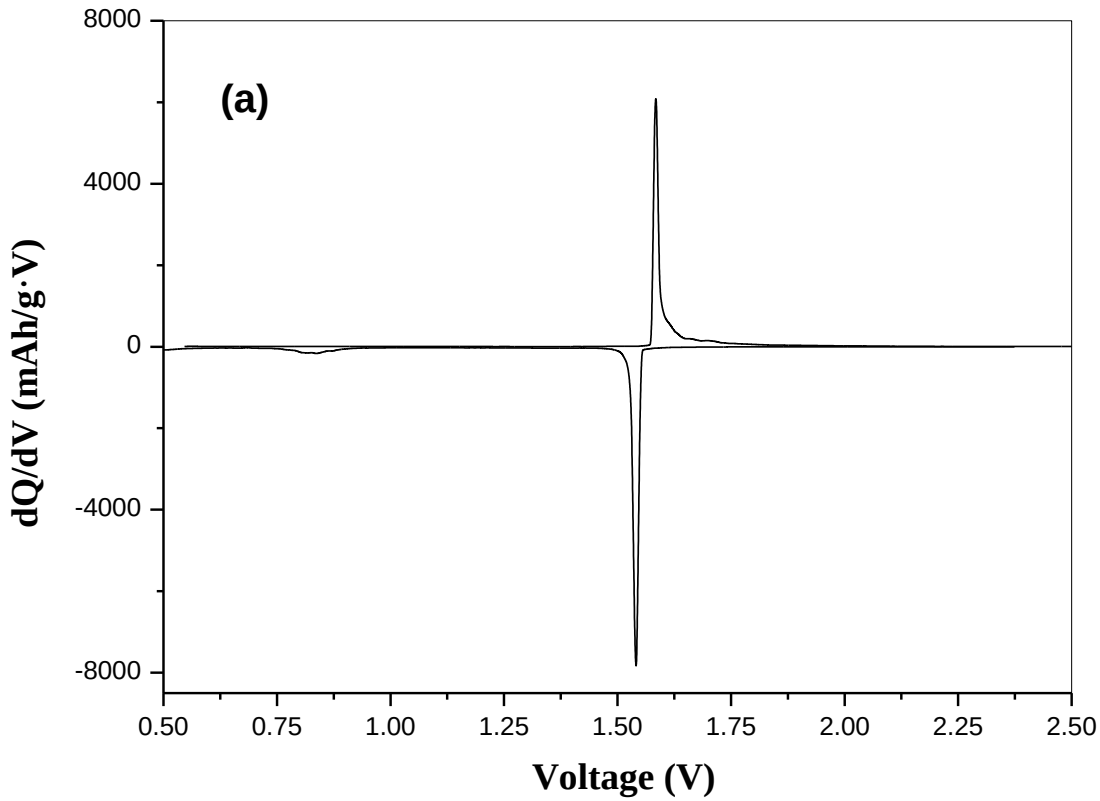

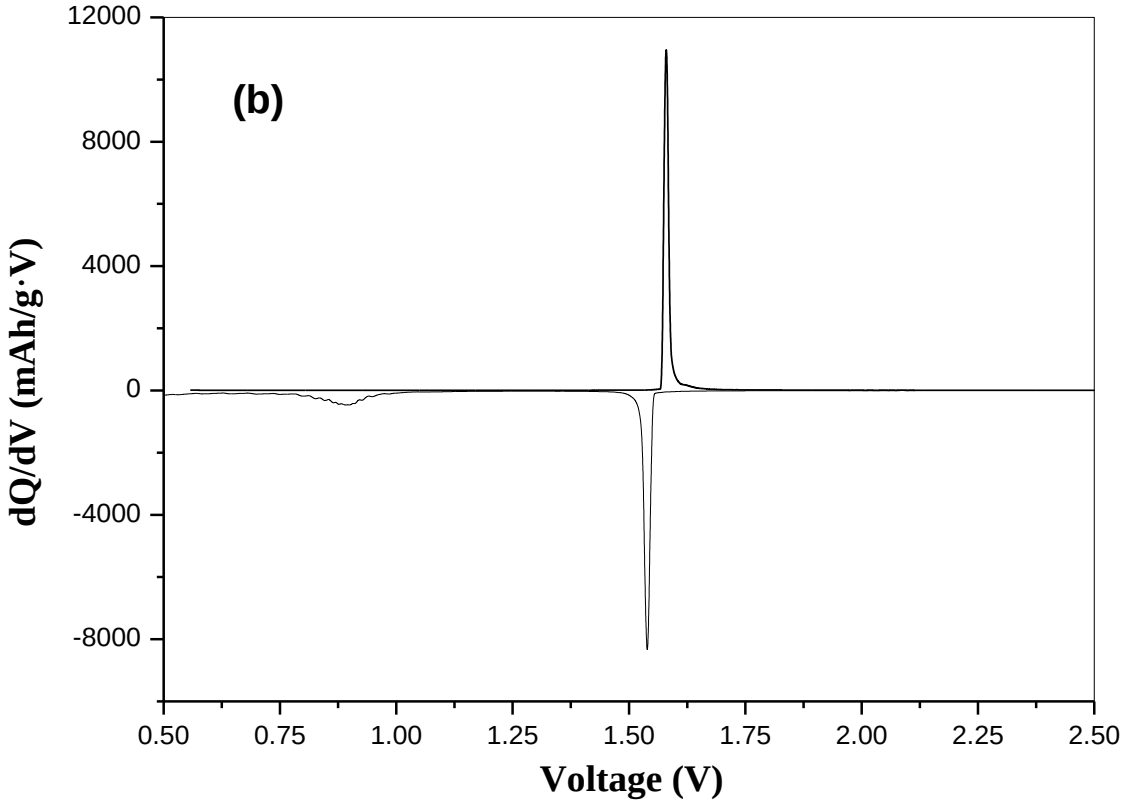
(b)
12000
8000
4000
0
-4000
-8000
dQ/dV (mAh/g·V)
0.50
0.75
1.00
1.25
1.50
1.75
2.00
2.25
2.50
Voltage (V)

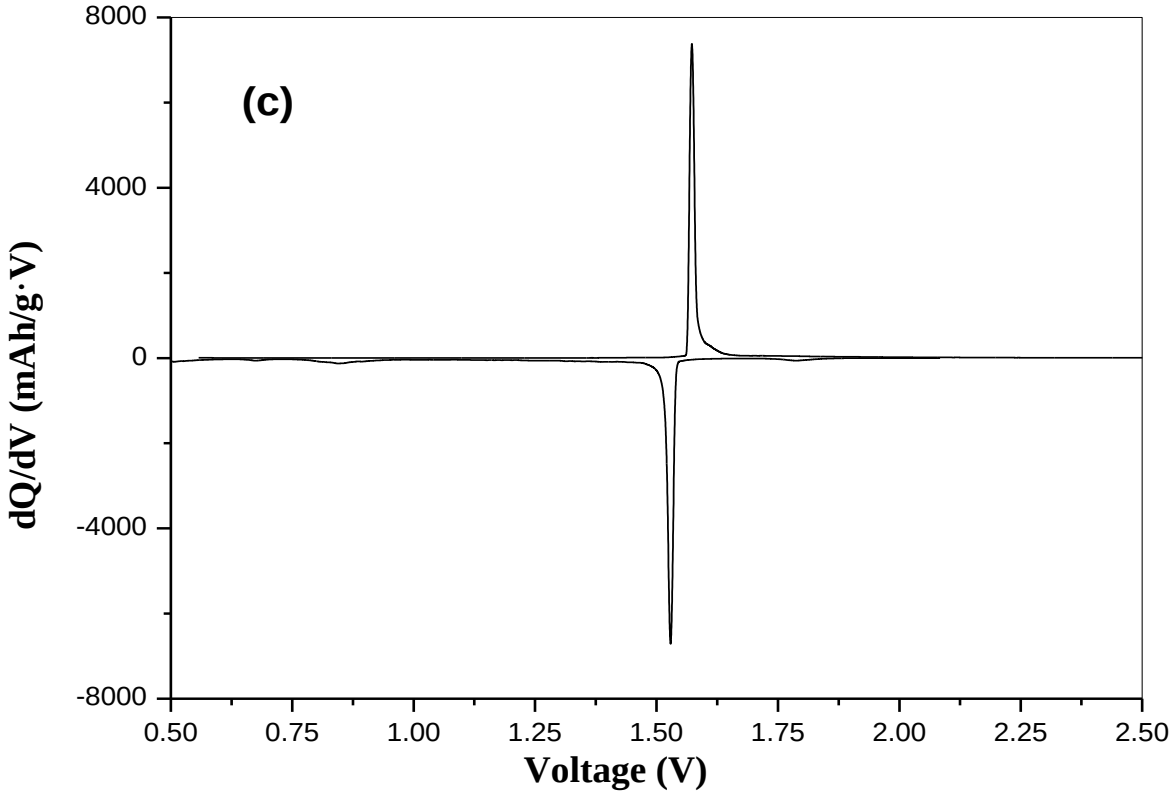
(c)
8000
4000
0
-4000
-8000
dQ/dV (mAh/g·V)
0.50
0.75
1.00
1.25
1.50
1.75
2.00
2.25
2.50
Voltage (V)

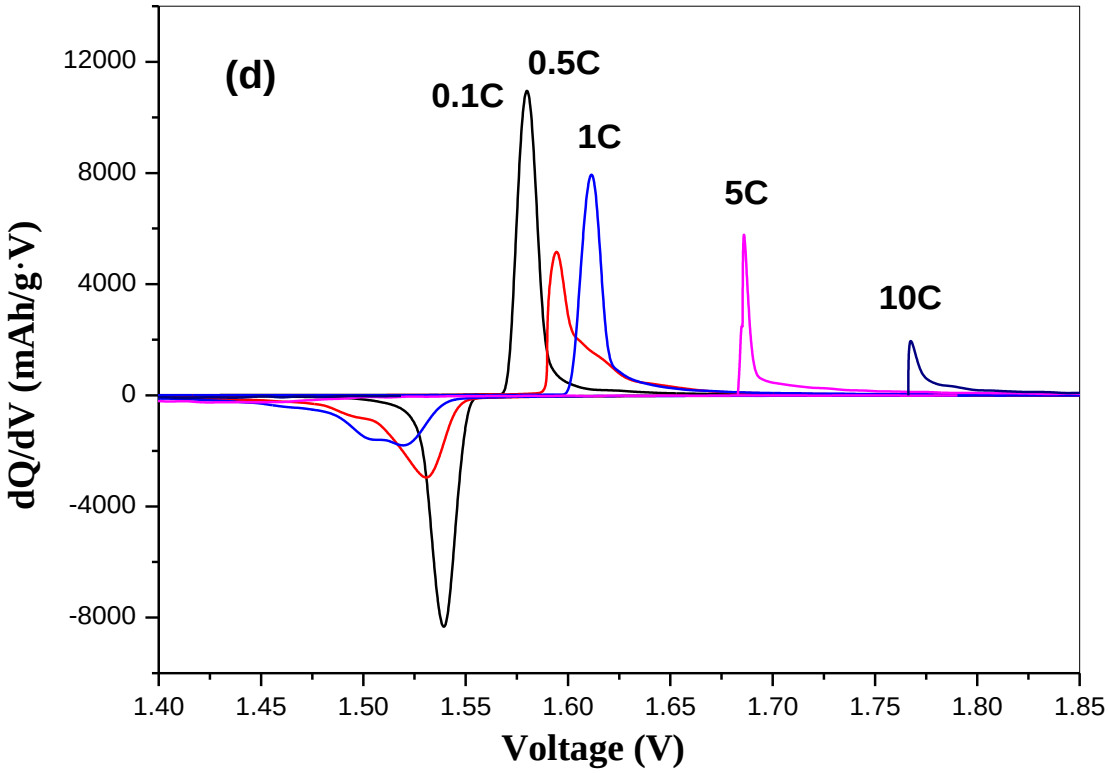

Figure 5. Differential curves of the three samples between 0.5 and 2.5 V. (a) LTO/SP at 0.1C; (b) LTO/BP-2000 at 0.1C; (c) LTO/VGCF at 0.1C; (d) LTO/BP-2000 from 0.1 to 10C

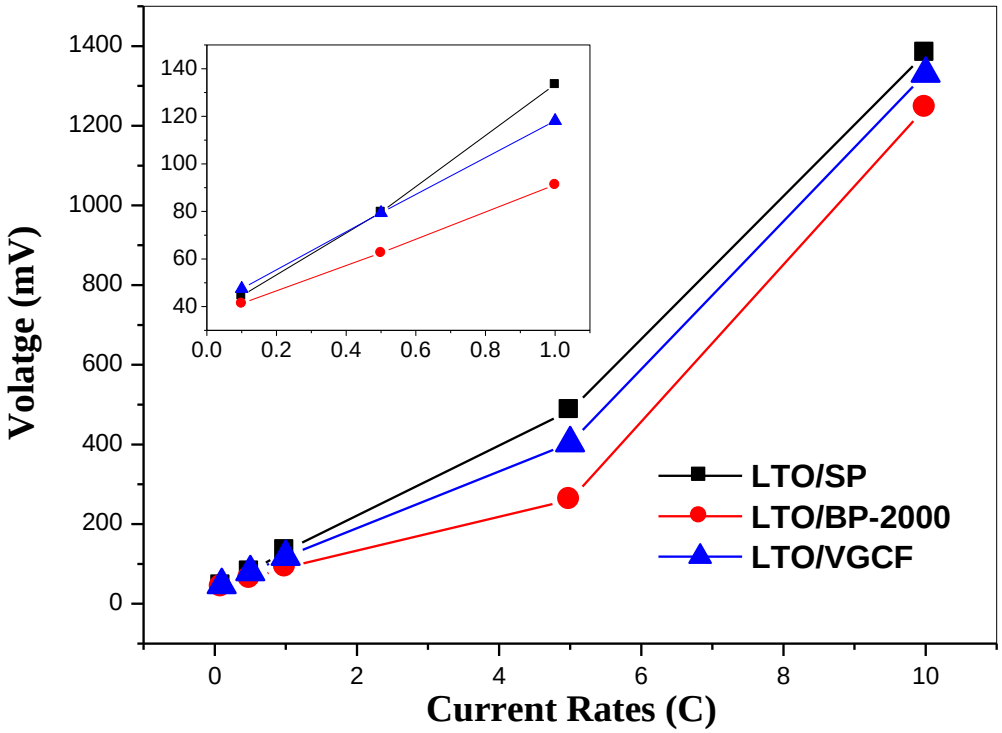

Figure 6. Potential difference between the redox peaks of LTO/C composites

The difference of the peak magnitude is relevant to the capacity, thus the surface area of carbon: the sample with BP-2000 shows the most obvious peak and that with VGCF shows the least peak. The differential curves of LTO/BP-2000 at different current densities are shown in Fig 5 (d) to analyze the effects of current density on the performance of LTO/C composite. It can be observed that although the redox peaks decrease with the increasing current density due to polarization, the reduction peaks (insertion reaction) disappear more clearly than the oxidation peaks (extraction reaction). This phenomenon indicates that the capacity of LTO at high rate mainly depends on the insertion process.

Potential interval between the oxidation peak and the reduction peak is usually used to examine the electrochemical reversibility of electrode material, the potentials between redox peaks of three samples change with current density at 0.1-5C are shown in Fig 6. The data of 10 C did not shown in the figure due to the plateau is not obvious. It can be seen that the potential difference shows a linear characteristic due to the increasing of the polarization. The order is in accordance to the change of the reversible capacity shown in Figure 4.

4. CONCLUSIONS

The $Li_4Ti_5O_{12}$ with 5% Super-P, BP-2000, VGCF was synthesized by a simple solid-state reaction, respectively. The roles of the added conductive carbon relate closely to their characteristics. The $Li_4Ti_5O_{12}$ with 5wt.% BP-2000 exhibits the best electrochemical performance due to great surface area. The capacity retention and rate performance of LTO/VGCF are better than that of LTO/SP at high current rates due to its three-dimensional conductive network among the isolated aggregated-particles. The result shows the specific surface area, the morphology of the conductive carbon affect the rate performance of LTO/C composite.

ACKNOWLEDGEMENT
The authors thank the financial support from the National Natural Science Foundation of China (No. 20903014), Doctoral Fund of Shandong Province (No. BS2010CL001), the Project of Science and Technology Development Planning of Shandong Province (no.2011YD02088) and Binzhou City (no.2011ZC0305) and Binzhou University (no.BZXYG1009).

References

1. G. J. Wang, J. Gao, L. J. Fu, N. H. Zhao, Y. P. Wu, T. Takamura, *J. Power Sources*, 174 (2007) 1109.
2. J. Gao, J. R. Ying, C. Y. Jiang, C. R. Wan, *J. Power Sources*, 166 (2007) 255.
3. T. Ogihara, M. Yamada, A. Fujita, S. Akao, K. Myoujin, *Mater Res Bull*, 46 (2011) 796.
4. X. B. Hu, Z. J. Lin, K. R. Yang, Z. H. Deng, J. S. Suo, *J. Alloys Compd*, 506 (2010) 160.
5. Y. Wang, H. Liu, K. Wang, H. Eiji, Y. Wang, H. Zhou, *J. Mater Chem*, 19 (2009) 6789.
6. F. Gu, G. Chen, *Int. J. Electrochem. Sci.*, 7 (2012) 6168.
7. J. Wang, X. M. Liu, H. Yang, X. D. Shen, *J. Alloys Compd*, 509 (2011) 712.
8. B. Li, F. Ning, Y. B. He, H. Du, Q. H. Yang, J. Ma, F. Kang, C. T. Hsu, *Int. J. Electrochem. Sci.*, 6 (2011) 3210.

9. H. Liu, Y. Feng, K. Wang, J. Y. Xie, *J. Phys. Chem. Sol*, 69 (2008) 2037.
10. J. Gao, C. Y. Jiang, C. R. Wan, *Ionics*, 16 (2010) 417.
11. L. X. Yang, L. J. Gao, *J. Alloys Compd*, 485 (2009) 93.
12. A. Guerfi, S. Sévigny, M. Lagacé, P. Hovington, K. Kinoshita, K. Zaghib, *J. Power Sources*, 119-121 (2003) 88.
13. X. D. Zheng, C. C. Dong, B. Huang, M. Lu, *Ionics*, DOI:10.1007/s11581-012-0767 -z.
14. T. F. Yi, L. J. Jiang, J. Liu, M. F. Ye, H. B. Fang, A. N. Zhou, J. Shu, *Ionics*, 17 (2011) 799.
15. H. Ge, N. Li, D. Y. Li, C. S. Dai, D. L. Wang, *J. Phys. Chem. C*, 113 (2009) 6324.
16. J. B. Goodenough, *Acc. Chem. Res*, DOI:10.1021/ar2002705.
17. M. Winter, P. Novak, J. Monnier. *J Electrochem Soc*, 145 (1998) 428.
18. Z. Ogumi and M.Inaba, in: W.A. van Schalkwijk, B. Scrosati (Eds.), *Advances in Lithium-Ion Batteries*, Kluwer Academic/Plenum Publishers, New York (2002).